JOURNAL OF CATALYSIS 93, 1–22 (1985)

The Characterization of Carbonaceous Species on Ruthenium Catalysts with ^{13}C Nuclear Magnetic Resonance Spectroscopy

T. M. DUNCAN,* P. WINSLOW,† AND A. T. BELL†

*AT&T Bell Laboratories, Murray Hill, New Jersey 07974,, and †Materials and Molecular Research Division, Lawrence Berkeley Laboratory and Department of Chemical Engineering, University of California at Berkeley, Berkeley, California 94720

Received August 24, 1984; revised December 4, 1984

^{13}C Nuclear magnetic resonance (NMR) spectroscopy has been applied to the study of carbon species deposited on supported and unsupported ruthenium catalysts during CO hydrogenation. Four forms of nonoxygenated carbon on the substrate have been identified, designated C_α, C_{β_1}, C_{β_2}, and unreactive carbon. Correlation of isotropic shifts, nuclear dipolar interactions, and anisotropy of chemical shielding leads to a description of each carbon species. C_α is interpreted as carbidic carbon atoms distributed in a variety of sites located on or below the metal surface. C_{β_1} and C_{β_2} are alkyl groups attached to the catalyst and are differentiated by their relative mobilities and interconversion to other forms. C_{β_1} reorients at room temperature but the motion is quenched at 100 K. C_{β_2} is motionally averaged at 110 K and is selectively depleted by purging the catalyst with an inert gas. The unreactive carbon has a ^{13}C NMR spectrum similar to that of turbostratic graphite. The relationships of the different carbon species to each other are discussed.

I. INTRODUCTION

Recent transient-response studies have shown that during CO hydrogenation two forms of nonoxygenated carbon exist on silica-supported ruthenium (Ru/SiO_2) (*1*) and ruthenium powder (*2*) catalysts. The ^{13}C nuclear magnetic resonance (NMR) spectra of these two reactive forms of carbon adsorbed on Ru/SiO_2, as well as the spectra of unreactive deposits have been described recently (*3*). We report here a detailed characterization with ^{13}C NMR spectroscopy of carbon adsorbed on Ru/SiO_2 and Ru powder. Specifically, we present evidence for two types of alkyl species on the catalyst and discuss the chemical structure, mobility, and spatial distribution of each species.

The presence of two forms of carbon adsorbed on Ru/SiO_2 were identified by transient-response method through differences in their reactivity with hydrogen to form methane (*1*). It was determined that the highly reactive species, C_α, is formed by the dissociation of CO independent of the presence of hydrogen and is the principal precursor to methane. The steady-state coverage of C_α, which is readily achieved after the reaction is begun, determines the rate of methanation. It was concluded that the less-reactive form, C_β, is formed from C_α in the presence of hydrogen and accumulates to amounts many times that of C_α. It was also shown that C_β can be reconverted to C_α by purging the reactor with an inert gas at reaction temperatures. The C_α and C_β forms of carbon have also been identified on Ru powder (*2*). Here again, C_α was observed to reach a steady-state level shortly after onset of the reaction, whereas C_β accumulated progressively on the catalyst. From H_2–D_2 tracer experiments, it was determined that the C_β species on Ru powder resembles alkyl groups, in that its H-to-C ratio lies between 1.8 and 2.4.

The inherent features of NMR spectroscopy make it well suited for the characterization of nonoxygenated carbon (*4*). For example, the amount of carbon in a sample is directly proportional to the spectral in-

0021-9517/85 $3.00

tensity. Second, shifts of the NMR absorptions reflect the character of local electrons (*5, 6*); conduction electrons shift NMR peaks to higher energies via the *s*-state hyperfine interaction between the electron spin and the nuclear spin, known as the Knight shift. The induced angular momentum of paired electrons in bonding orbitals creates a magnetic field that also shifts the NMR peak; this interaction is termed chemical shielding. The isotropic shifts of ^{13}C NMR peaks allow one to interpret the species in terms of general chemical classes (*i.e.*, paraffinic, carbonyl), by comparison with compilations of organic (*7*) and organometallic (*8–10*) compounds. Third, the NMR absorption is broadened by dispersion in magnetic fields at corresponding nuclei of different species, caused by orientational anisotropy of the interactions with electrons and by nuclear dipolar couplings. The anisotropy of the chemical shielding provides a distinctive fingerprint to identify specific chemical structures within a chemical class. The nuclear dipole–dipole interaction is determined by local densities and mobilities of nuclear spins. However, analysis of the spectral broadening is contingent on the resolution of these two interactions. Fortunately, the contributions from each effect can be separated because the phenomena are inherently different; the chemical shift anisotropy is inhomogeneous and the nuclear dipolar coupling is homogeneous. Herein lies a useful feature of NMR spectroscopy; the resonators (nuclear spins) are more strongly coupled to the excitation (radio-frequency electromagnetic pulses) than to the environment (*11*). That is, for ^{13}C NMR, the rf excitations last only a few microseconds, whereas it typically requires milliseconds for the energy to distribute among the spins (via homogeneous interactions) and it requires seconds for the spins to equilibrate with the lattice. The time constant for the thermal equilibration of the spins with the lattice is T_1, the spin–lattice time. The redistribution of energy among nuclear spins is described by the time constant T_2, the spin–spin relaxation time.

The applicability and potential of ^{13}C NMR spectroscopy has been demonstrated by the report of the spectra of C_α, C_β, and unreactive carbon on Ru/SiO_2 (*3*). The spectral features were assigned on the basis of changes in the spectra that accompanied changes in relative amounts of C_α and C_β, as observed in transient-response studies. In the present investigation we have extended our initial studies of Ru/SiO_2 and have characterized the forms of carbon on Ru powder. The results reported here support the spectral assignments for C_α and unreactive carbon proposed previously (*3*), but an alternate description of C_β is proposed.

II. EXPERIMENTAL PROCEDURES

A. Materials

Two types of ruthenium catalysts were studied: ruthenium dispersed on silica at a loading of 4.3 wt% and Ru powder. Ru/SiO_2 catalysts were prepared by incipient-wetness impregnation of silica (Cab-O-Sil HS-5) with an aqueous solution of $RuCl_3 \cdot 3H_2O$ (*1*). Freshly prepared catalysts were reduced in flowing D_2 (or H_2) at 673 K for 2 hr, which typically resulted in a dispersion of 27%, determined by H_2 chemisorption at 373 K. Ru powder (99.9%) was obtained from MacKay A.D., Inc. Following reduction for 12 hr at 463 K in flowing D_2 (or H_2), the dispersion of Ru powder was 0.35 ± 0.05% (*2*).

To interpret the ^{13}C relaxation times (T_1 and T_2), it was necessary to know the amount of paramagnetic impurities in the catalysts. Thus, iron contents of catalysts at various stages of preparation were determined by spark-source mass spectrometry. The silica contained only 10 ppm Fe by weight. However, the iron content increased markedly with the addition of ruthenium; the dried particles of $RuCl_3$ on silica, prior to reduction in H_2, contained 100 ppm Fe. The Fe content of another Ru/SiO_2

sample after reduction was 500 ppm, although this high level may have been an anomaly since a third sample was found to contain 100 ppm of Fe after reduction and methanation. The Ru powder as-received contained 200 ppm Fe; the Fe level remained unchanged after reduction and methanation. The Fe contents are subject to errors of ±30%. It is important to note that while the level of Fe impurities seems high, the influence of Fe on the NMR spectra is negligible. The measured values of ^{13}C T_1's were routinely between 1 and 3 sec, much longer than the few milliseconds that would have been expected if paramagnetic impurities were present at level of over 100 ppm. This suggests that most impurity Fe present in the samples is nonparamagnetic. Also consistent with this conclusion is the observation that the T_1 of ^{29}Si in a Ru/SiO_2 sample was 51 ± 5 sec.

For reference, a sample of ^{13}C-enriched (91%) turbostratic graphite (*12, 13*) was obtained from Prochem. Although marketed as "amorphous carbon," X-ray diffraction revealed that the compound is ordered, in agreement with studies of similar samples (*14*). That is, the planar hexagonal layers are clearly defined but lack long-range (greater than 100 Å) stacking registry. The turbostratic graphite was outgassed to a pressure of 10^{-5} Torr at 673 K over a period of 4 days.

H_2, D_2, and ^{12}CO were purified with techniques described in Refs. (*1, 2*). ^{13}CO (99% ^{13}C) was obtained from Liquid Carbonic and was used without further purification.

B. Apparatus

The reactor used for NMR samples is a 10-mm-o.d. Pyrex tube in the shape of a U with ends fused to copper tubes. The catalysts are contained in the base of the U, which is a straight section approximately 25 mm in length. The gas handling and analysis systems are identical to those used previously (*1, 2, 15*). The gas-handling manifold is designed to produce step-function changes in isotopic (or overall) composition of the gas mixture fed to the reactor. Thus, for example, the composition of the feed gas can be switched from H_2 (or D_2) and ^{13}CO to a composition of H_2 (or D_2) and ^{12}CO. The response of the reactor is monitored by analysis of the effluent with a quadrupole mass spectrometer. A microcomputer is used to switch the composition of the feed gas and to control the mass spectrometer.

C. Preparation of Samples for NMR Studies

The preparation of samples for analysis by ^{13}C NMR spectroscopy was carried out using the gas delivery sequence shown in Fig. 1. The catalyst was first reduced in D_2 (or H_2) and then exposed to a mixture of D_2

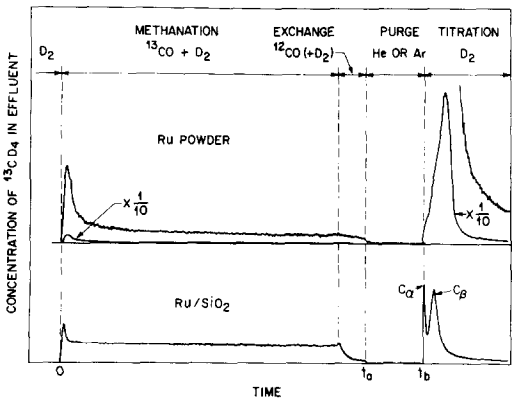

FIG. 1. Sequence of events with corresponding curves for the rate of production of $^{13}CD_4$ in the transient-response experiment used to prepare catalyst samples for analysis with NMR spectroscopy. As discussed in detail elsewhere (*1*), at steady-state methanation the carbon on the catalyst is predominantly C_β. *Steady-state* samples are obtained by quenching the reaction at time t_a, after exchanging ^{13}CO for ^{12}CO. Purging the reactor with an inert gas converts a portion of the C_β to C_α. Quenching the reactor after the purge in He or Ar (time t_b) yields *converted* samples. Finally, titrating the catalyst with D_2 for extended periods depletes the reactive forms of carbon. Samples sealed after extended reaction with hydrogen are termed *titrated*. Some samples were prepared using the above scheme, but with H_2 substituted for D_2. For reference, the steady-state rates of methanation for the two transients shown above are 7.8×10^{-8} (g mol $^{13}CD_4$) $(sec)^{-1}$ $(g\ cat)^{-1}$ for the Ru powder (top) and 1.9×10^{-7} (g mol $^{13}CD_4$) $(sec)^{-1}$ $(g\ cat)^{-1}$ for the Ru/SiO_2.

and ^{13}CO. After the rate of $^{13}CD_4$ formation has reached steady state, ^{13}CO was replaced with ^{12}CO for a short period of time (30 to 120 sec), to rapidly displace all the adsorbed ^{13}CO with ^{12}CO, leaving only nonoxygenated ^{13}C on the catalyst (*1*). Termination of the reaction after exchange (time t_a in Fig. 1) produces a *steady-state* sample in which the distribution of nonoxygenated carbon is representative of that occurring at the end of the period of steady-state reaction. For the Ru/SiO_2 catalyst this distribution consists mainly of C_β with relatively small amounts of C_α (*1*). To enhance the C_α signal for NMR studies, as well as to study the interconversion of surface species, *converted* samples are prepared by purging with an inert gas (He or Ar) after the $^{13}CO/^{12}CO$ exchange. That is, *converted* samples are quenched at time t_b in the sequence diagramed in Fig. 1. Finally, flowing hydrogen through the reactor after methanation, exchange, and purge removes the reactive carbon from the surface and yields samples referred to as *titrated*. Note that the $^{13}CD_4$ transient observed during titration of the Ru/SiO_2 shown in Fig. 1 provides a measure of the relative amounts of C_α and C_β on the catalyst after conversion; the first peak is due to the direct reaction of C_α, whereas the second peak is the result of C_β converting to species which subsequently react with hydrogen to form methan (*1*). The $^{13}CD_4$ transient observed during titration of Ru powder catalysts is fundamentally different in two respects: the peak is over an order of magnitude larger and there is less resolution between the C_α and C_β peaks. Table 1 lists the specific conditions used to prepare each of the eight samples examined during this study.

To permit analysis of the samples with ^{13}C NMR spectroscopy it was necessary to quench the reaction occurring on the catalyst surface. This was done in the following manner: the reactor was raised from the fluidized sand bath, cooled to room temperature with forced-air convection, and then

TABLE 1

Description of Ruthenium Catalyst Samples

Sample[a]	Sample wt. (g)	Catalyst activity[b]	Sample preparation conditions						
			Reaction temp. (°K)	Methanation period		Exchange period		Purge duration (sec)	Titration duration (min)
				Reactants[c] (Torr)	Duration (sec)	Reactants[c] (Torr)	Duration (sec)		
A. Ru/SiO_2; Steady state; D_2	0.28	2.9×10^{-7}	443	D_2 (580) ^{13}CO (90)	300	^{12}CO (90)	120	Quench in ^{12}CO	—
B. Ru/SiO_2; Steady state; D_2	0.34	$\sim 6 \times 10^{-7}$	463	D_2 (360) ^{13}CO (200)	300	D_2 (360) ^{12}CO (200)	30	Quench in ^{12}CO	—
C. Ru/SiO_2; Steady state; H_2	0.26	1.5×10^{-7}	443	H_2 (580) ^{13}CO (90)	900	^{12}CO (90)	120	Quench in ^{12}CO	—
D. Ru/SiO_2; Converted; D_2	0.36	$\sim 3 \times 10^{-7}$	463	D_2 (360) ^{13}CO (200)	300	D_2 (360) ^{12}CO (200)	30	120	Quench in Ar
E. Ru/SiO_2; Converted; H_2[d]	0.31	—	463	H_2 (360) ^{13}CO (200)	300	H_2 (360) ^{12}CO (200)	30	120	Quench in Ar
F. Ru/SiO_2; Titrated; D_2	0.34	$\sim 5 \times 10^{-7}$	463	D_2 (360) ^{13}CO (200)	300	D_2 (360) ^{12}CO (200)	30	0	120; Quench in D_2
G. Ru; Steady state; D_2	1.70	7.8×10^{-8}	443	D_2 (150) ^{13}CO (50)	300	^{12}CO (50)	120	Quench in ^{12}CO	—
H. Ru; Steady state; H_2	0.94	2.4×10^{-8}	443	H_2 (150) ^{13}CO (50)	900	^{12}CO (50)	120	Quench in ^{12}CO	—
I. Ru/SiO; CO	0.33	—	[e]	—	—	—	—	—	—
J. Ru/SiO_2; CO_2	0.33	—	[e]	—	—	—	—	—	—

[a] Silica-supported ruthenium catalysts contain 4.3 wt% Ru; see Experimental Procedures and Fig. 1 for a description of the nomenclature.
[b] Defined as the rate of production of methane after 300 sec of methanation (g mol methane) $(sec)^{-1}(g\ cat)^{-1}$.
[c] He (or Ar) used as carrier gas to bring total pressure to 760 Torr; total flow rate = 152 std $cm^3\ min^{-1}$.
[d] Sample E was prepared from a Ru/SiO_2 catalyst previously used for methanation, then reduced at 673 K.
[e] Gases adsorbed at room temperature.

flow through the reactor was stopped. We observed that quenching in this manner does not cause irreversible changes in the adsorbed species. That is, if the experiment is resumed with a quenched sample by reheating the sample and restarting the flow, the observed transient is indistinguishable from those of unquenched, uninterrupted samples. We also observed that quenched samples are stable at room temperature, with respect to the ^{13}C NMR spectra. The ^{13}C NMR spectra of a *steady-state* sample (A) and a *converted* sample (E) were unchanged when measured 1 day after preparation and 6 weeks later.

After quenching the reaction, the final step is to disconnect the reactor from the gas manifold, as follows. The inlet and outlet copper tubes are pinched closed and the flattened sections are coated with UHV epoxy. Before the epoxy hardens, the flattened sections of the tubes are severed from the gas manifold by fatigue-stressing. Any leaks through the mechanical seals are automatically plugged with the epoxy.

The catalyst samples prepared with ^{13}C-enriched reactive intermediates are saturated with natural-abundance CO and, perhaps, some CO_2 formed by disproportionation. To complement the ^{13}C NMR studies of nonoxygenated carbon, it was useful to measure the spectra of two adsorbed oxygenated forms: CO and CO_2. Two samples of Ru/SiO_2 were reduced in D_2 at 673 K for 2 hr, cooled to room temperature and outgassed. Sample I was exposed to 200 Torr of ^{13}CO for 5 min, purged with Ar for 5 min, then sealed. Sample J was exposed to $^{13}CO_2$, allowed to equilibrate for 14 hr, and was sealed under a pressure of 6.1 Torr of $^{13}CO_2$. Pressure–volume measurements indicated that sample J adsorbed 24 μmol of $^{13}CO_2$.

D. Measurement of ^{13}C NMR Spectra

The ^{13}C NMR experiments were performed on a Bruker CXP-200 spectrometer, operating at 50.34 MHz. The procedure for inserting a sample tube into the NMR probe is unorthodox and warrants discussion. One end of a U-shaped reaction tube is inserted through the NMR coil (desoldered from the circuitry at one end) until the catalyst section is centered in the coil. After the coil is reconnected, the electrical impedance, disrupted by deformation during insertion, is restored by compressing or expanding the coil, without adjusting the tunable components of the probe. The lengths of the 90° pulses were rechecked with ^{13}C-enriched reference samples after inserting and removing each catalyst sample and were found to require corrections of less than 10%, which contributes less than 1% error to the integrated areas of the spectra. The resolution in the spectra is determined only by the stability and homogeneity of the static magnetic field and was therefore unaffected by deformation of the sample coil.

Spectra were measured by Fourier-transforming the nuclear precession observed immediately after a 90° pulse (free-induction decay) and observed as echoes stimulated by a 180° pulse (spin–echo). The broad, weak ^{13}C nuclear signal from the submonolayer coverages of carbon species required prolonged accumulation of decays (10,000 to 64,000 scans). Consequently, it is critical to eliminate spurious signals from the excitation pulses; an add–subtract method was used here. The free-induction decays were successively acquired from (90°_x–observe) and (180°_x–τ–90°_x–observe) sequences, with alternate adding and subtracting of signals. Similarly, the spin–echo experiment was composed of alternate (90°_x–τ–180°_x–τ–observe) and (90°_x–τ–180°_x–τ–observe) pulse sequences.

The spin–lattice (T_1) and spin–spin (T_2) relaxation times were determined from the results of saturation–recovery and spin–echo pulse sequences, respectively (*4*, *5*). Because the ^{13}C NMR spectra typically require about 8 hr each, T_1 and T_2 were calculated from the results of three to five spectra. Consequently, the values reported for the relaxation times are estimates, which is

usually sufficient for the information required in this study. That is, T_1 was measured primarily to assure the accuracy of the ^{13}C spin counts based on the spectral intensities. Also, the saturation–recovery and spin-echo experiments were performed to check for nonuniform values of T_1 and T_2, as revealed by a nonlinear plot of the spectral intensities versus the delay times or as revealed by changes in the spectral width and position. As will be demonstrated, the observation of nonuniform values of T_1 or T_2 can suggest the presence of multiple, overlapping components.

Different procedures were required to measure the ^{13}C NMR spectra on the Ru/SiO_2 and Ru-powder catalysts because the samples have different electrical conductivities. Since ruthenium dispersed on silica is present as particles approximately 30–100 Å in diameter (*16*) the sample behaves as an insulator. The length of a 90° pulse for Ru/SiO_2 samples is 2.6 μsec which provides uniform excitation over a range of 200 kHz (4000 ppm). Ruthenium particles in the unsupported powder are about 50 μm in diameter and although the particles are smaller than the skin depth of the rf radiation, the bulk conductivity of the powder markedly changes the impedance of the NMR probe. With Ru powder samples in the probe, approximately 80% of the incident rf voltage is reflected and accordingly the length of a 90° pulse increases to 13 μsec. The reflected power requires about 100 μsec after a pulse to dissipate which precludes the observation of free-induction decays immediately after a 90° pulse. As a consequence, the NMR spectra of Ru-powder catalysts were obtained from spin–echoes.

Although the bulk conductivity of Ru-powder catalysts perturb the probe impedance, the bulk susceptibility does not detectably shift the positions or broaden the ^{13}C NMR peaks. For example, the ^{13}C NMR spectrum of a sample of Ru powder saturated with tetramethylsilane (TMS) is indistinguishable from that of the neat liquid; the TMS in the interparticle voids resonates at 1.1 ± 1.0 ppm relative to the neat liquid.

The ^{13}C NMR spectra are plotted on the δ scale for chemical shifts, relative to TMS, such that downfield lies to the left (*i.e*, C_6H_6 is at 128.7 ppm and CS_2 is at 192.8 ppm). For each sample, the frequency range between 1600 and -800 ppm was examined, although only the portion between 800 and -400 ppm are reported here. The spectral intensities were calibrated with samples of SiC and ZrC.

III. EXPERIMENTAL RESULTS

A. Carbon Coverages Measured by Transient-Response Titrations

Before sealing the catalyst samples for study with NMR, the amounts of C_α and C_β on each catalyst, given in Table 2, were determined by observing the $^{13}CD_4$ (or $^{13}CH_4$) mass signal caused by titrating the sample with D_2 (or H_2), as described previously (*1, 2*). Each catalyst was titrated at a point in the gas-delivery sequence (see Fig. 1) that corresponded with the point at which the sample was later quenched for NMR study. For example, the *steady-state* samples (A–C, G–H) were titrated with hydrogen after methanation and $^{13}CO/^{12}CO$ exchange (time t_b in Fig. 1). The experimental parameters given in Table 1, were the same during the initial measurement of the transients and during the preparation of the NMR samples. The total amount of reactive carbon on a sample was determined by integrating the amount of $^{13}CD_4$ (or $^{13}CH_4$) observed during the titration period as shown in Fig. 1. The distribution of carbon between C_α and C_β was determined by separating peaks with a tangential–baseline method. The accuracy in the total amount of reactive carbon is ±15%. Since C_β accounts for most of the transient, it can also be determined to ±15%. Resolving the smaller C_α transient is difficult, particularly for Ru powder, and the accuracies of the C_α amounts are ±30%.

TABLE 2

Coverages of Carbon Species on Ruthenium Catalysts

Sample	Surface Ru[a] (10^{-6} g mol)	Titration with hydrogen[b,c]			^{13}C NMR integrated areas[b]			
		C_α	C_β	Total	C_α	$C_{\beta_1} + C_{\beta_2}$	Unreactive	Total
A. Ru/SiO_2; Steady state; D_2	32	2.0	8.3	10.3	3.5	18.5	0	22.
B. Ru/SiO_2; Steady state; D_2	39	2.4	46.	48.	1.5	27.	0.5	29.
C. Ru/SiO_2; Steady state; H_2	30	2.1	13.	15.	6.	29.	0	35.
D. Ru/SiO_2; Converted; D_2	43	~7.	~7.	14.	8.	12.	10.	30.
E. Ru/SiO_2; Converted; H_2	36	—	—	—	8.	3.	5.5	16.5
F. Ru/SiO_2; Titrated; D_2	39	2.4	40.	42.[d]	0	0	7.	7.
G. Ru; Steady state; D_2	59	~4.3	264.	268.	18	3	1.	22.[e,f]
H. Ru; Steady state; H_2	33	<4.	230.	234.	19.5	2	0.5	22.[e,f]
I. Ru/SiO_2; CO	38	—	—	—	—	—	—	32.[f]
J. Ru/SiO_2; CO_2	38	—	—	—	—	—	—	23.[f]

[a] Approximate values estimated from typical dispersions of 27% for silica-supported Ru (*1*) and 0.35% for particulate Ru (*2*).

[b] In 10^{-6} g mol of ^{13}C.

[c] Relative amounts of C_β and C_α are approximate; see Refs. (*1, 2*).

[d] Titrated after steady-state methanation; quantities do not correspond to state of sample when measured by NMR.

[e] Minimum value; metallic character of samples may have attenuated NMR signal.

[f] Minimum value; T_1 not measured.

B. ^{13}C NMR Spectra

1. Steady-state Ru/SiO_2 samples. The ^{13}C NMR spectra of Ru/SiO_2 samples quenched with *steady-state* coverages of nonoxygenated carbon (samples A–C) are shown in Figs. 2–5. These spectra contain two distinct features: an intense, relatively narrow, Lorentzian peak at about 20 ppm and a weaker, broader peak positioned downfield at about 400 ppm. In this section, we describe the subtle changes in these two spectral features that accompany variations in the specifics of the NMR experiment and the isotopic composition of the sample.

The two features in the ^{13}C NMR spectra of samples A, B, and C did not change in width or center of mass as in the interval between successive scans was varied. For example, Fig. 2 shows three ^{13}C NMR spectra of sample A measured with the saturation–recovery experiment. The width and center of the intense upfield peak are calculated by fitting to a Lorentzian lineshape; the peak has a half-width of 1.16 ± 0.03 kHz and is centered at 19 ± 1 ppm relative to TMS. The downfield peak in the spectra of Fig. 2, as well as the downfield peaks in all the spectra in this study, are generally better fit by Gaussian lineshapes. The half-width of the Gaussian fit to the downfield peak is 3.1 ± 0.3 kHz; the peak is centered at 390 ± 15 ppm.

The two features in the ^{13}C NMR spectra of sample A (Fig. 2) have different T_1's; the T_1 of the intense upfield peak is 3.3 sec and

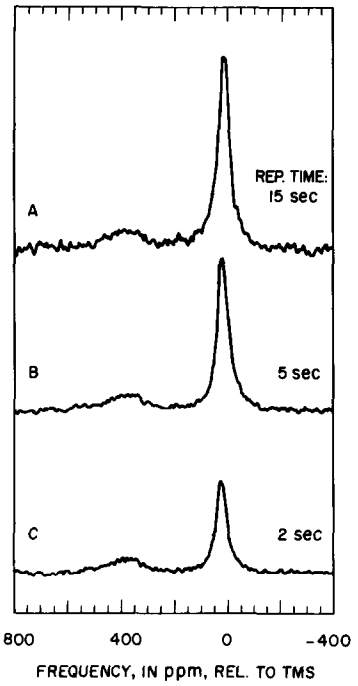

FIG. 2. Saturation–recovery study of a Ru/SiO_2 catalyst quenched after steady-state methanation (in D_2) and $^{13}CO/^{12}CO$ exchange (Sample A). The ^{13}C NMR spectra were measured at 295 K with delays of 15 sec (A), 5 sec (B), and 2 sec (C) between scans and are the accumulation of 10,000 scans (15 sec) to 40,000 scans (2 sec).

the T_1 of the weaker downfield peak is 1.1 sec. Moreover, the upfield peak has a uniform value of T_1; the semilogarithmic plot of the integrated area versus the repetition time is linear. The weak intensity and short T_1 of the downfield peak do not afford a conclusion as to the uniformity of T_1. The calibrated integrated area of spectrum A in Fig. 2 indicates the sample contains 2.2×10^{-5} g mol of ^{13}C nuclei and the upfield peak accounts for 84% of the spectral intensity.

The upfield peak in Fig. 2 has a Lorentzian shape, which suggests this species may be in motion, with a correlation time on the order of the inverse of the linewidth (1 msec). Indeed, the low-temperature study of sample A in Fig. 3 confirms that the lineshape is motionally narrowed at room temperature. That is, the line broadens as the temperature of the catalyst is lowered. Below 165 K, the increase in width as a function of temperature is more gradual and at 110 K the spectrum has broadened to a half-width of 3.1 ± 0.1 kHz. Although the spectra through 165 K are well represented by Lorentzian lineshapes, the spectra at lower temperatures exhibit slight deviations. Specifically, at 110 K the observed peak is too broad at the base and too narrow at the center, as compared to the best-fit Lorentzian function. Also, the upfield peak shifts upfield as the temperature is decreased; the peak is at 19 ± 1 ppm at 295 K, 14 ± 2 ppm at 165 K, and 10 ± 3 ppm at 110 K. Finally, the sharp feature that appears at ~180 ppm in the spectra at 130 and 110 K is interpreted as physically adsorbed ^{13}CO, which condenses from the gas phase in the sealed reactor.

The second *steady-state* sample, B, is

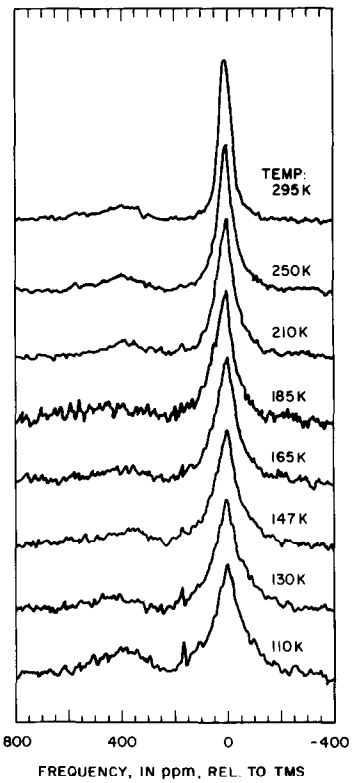

FIG. 3. Temperature dependence of ^{13}C NMR spectra of a Ru/SiO_2 catalyst quenched after steady-state methanation (in D_2) and $^{13}CO/^{12}CO$ exchange (Sample A). All spectra were acquired with a repetition time of 5 sec and represent about 3000 scans each.

similar to sample A, with two changes: the D_2 : ^{13}CO ratio was decreased from 6.4 : 1 to 1.8 : 1 and the reaction temperature was increased from 443 to 463 K. The ^{13}C NMR spectra of sample B are presented in Fig. 4; spectrum A may be compared directly with spectrum 2C. The upfield peak has a T_1 of 4.7 sec, a half-width of 1.10 ± 0.03 kHz, and is centered at 14 ± 1 ppm. The area of this peak accounts for about 95% of the total integrated area. The upfield peak represents 2.7×10^{-5} g mol of ^{13}C, as determined from the saturation-corrected intensity of a spectrum measured with a repetition time of 8 sec (not shown). Because the downfield peak is barely detectable in sample B, its spectral parameters could not be determined.

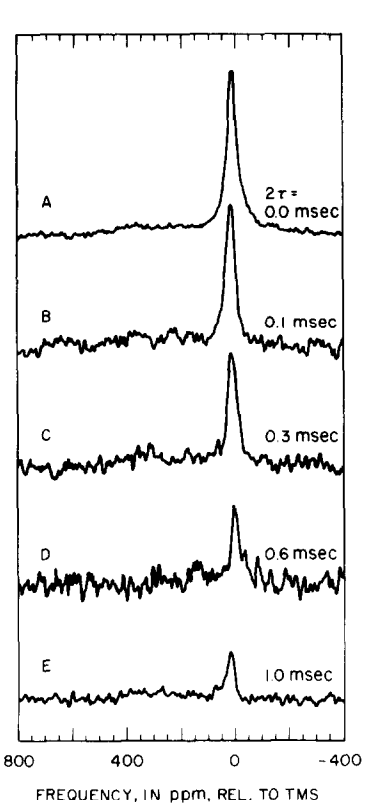

FIG. 4. Spin–echo study at 295 K of a Ru/SiO_2 catalyst quenched after steady-state methanation (in D_2) and $^{13}CO/^{12}CO$ exchange (Sample B). The ^{13}C NMR spectra were obtained from a free-induction decay (A) and from the echoes stimulated by a 180° pulse 0.1, 0.3, 0.6, and 1.0 msec after the 90° excitation. All spectra were acquired with a repetition time of 3 sec; the free-induction decay represents the accumulation of 52,800 scans and the echoes are the result of about 10,000 scans each.

For the spectra in Fig. 4, the logarithm of the spectral intensity decreases linearly as the delay to the echo (2τ) is increased, yielding a T_2 of 0.80 msec. Within experimental error (±3 ppm) the position of the peak does not shift as the echo delay is increased. However, the peak narrows slightly as the echo delay increases; the half-widths are 1.09, 0.92, 0.86, 0.83, and 0.73 kHz for the spectra observed with the echo delays of 0.0 (FID), 0.1, 0.3, 0.6, and 1.0 msec, respectively.

The third *steady-state* sample, C, is also similar to sample A, but with two changes: the catalyst was prepared with H_2 rather than D_2 and the methanation period was extended from 300 to 900 sec. The methanation period was lengthened to compensate for the depressed rate of formation of C_β in H_2 compared to D_2, caused by an isotope effect (*2*). Although the spectrum obtained from the FID (Fig. 5A), is similar to the corresponding spectrum 2A, there is a distinct difference in the shape of the upfield peak. Specifically, the base of the upfield peak has broadened to extend into the downfield peak. However, the upfield peak has not broadened uniformly, which is apparent in two ways. First, the upfield peak is no longer adequately represented by a Lorentzian lineshape. Rather, the simulation of the peak is improved by considering the sum of two Lorentzians. In contrast, the simulation of the upfield peaks of samples A and B were only marginally improved by considering a sum of two Lorentzians. A least-squares fit to the upfield peak yields the following results; a narrow component centered at 18 ± 2 ppm with a half-width of 1.23 ± 0.03 kHz and a broader component centered at 10 ± 4 ppm with a half-width of 3.9 ± 0.3 kHz. The fit was less sensitive to the relative areas of the two components, but a best fit was obtained at a 50 : 50 ratio of each. The second evidence that the upfield peak is composite is the variation in

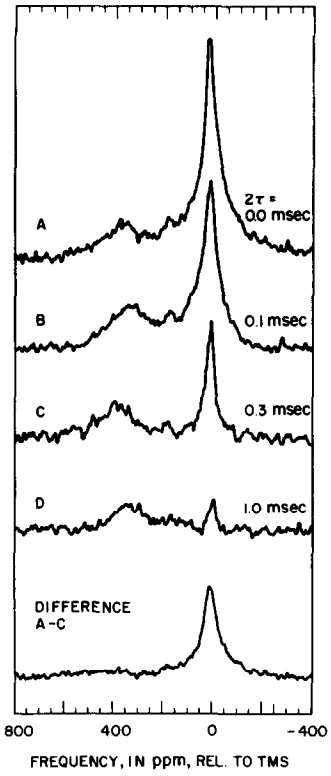

FIG. 5. Spin–echo study at 295 K of a Ru/SiO_2 catalyst quenched after steady-state methanation (in H_2) and $^{13}CO/^{12}CO$ exchange (Sample C). The ^{13}C NMR spectra were obtained from a free-induction decay (A) and from the echoes stimulated by a 180° pulse 0.1, 0.3, and 1.0 msec after the 90° excitation. All spectra were acquired with a repetition time of 5 sec and represent about 32,000 scans each.

linewidth with the spin–echo delay, shown in Fig. 5. For example, the spectrum that remains after a delay of 0.3 msec has a half-width of 0.85 kHz. The portion of the lineshape that decayed during the 0.3-msec delay, obtained by subtracting spectrum C from A, is a Lorentzian of half-width 2.9 kHz centered at 12 ppm. The average T_2 of the upfield peak of sample C is 0.26 msec. Decomposing each spectrum into a sum of two Lorentzian components yields a T_2 of 0.34 msec for the narrow component and a T_2 of 0.20 msec for the broader component; both components decay exponentially with echo time.

Sample C contains 3.5×10^{-5} g mol of ^{13}C, as calculated from the integrated area of spectrum A. Because the peaks in Fig. 5 are partially overlapped, it is more difficult to separate the relative contributions. We estimate that the downfield peak is centered at 380 ± 25 ppm and has a half-width of 4.4 ± 0.4 kHz. The intensity of the downfield peak decreases exponentially with time and has a T_2 of 2.3 msec, which is considerably longer than that of the upfield peak. As a result, the downfield feature in Fig. 5 retains over half its intensity even when observed as an echo at 1.0 msec.

2. Converted Ru/SiO_2 samples. Figures 6–8 contain the ^{13}C NMR spectra of Ru/SiO_2 catalysts quenched following the conversion of the steady-state coverage by purging with Ar or He to enhance the amount of C_α. Relative to the ^{13}C NMR spectra of samples with *steady-state* coverages (Figs. 2-5), the downfield peak at ~350 increases in intensity and there is considerable absorption in the region in the range 200 to 50 ppm. The upfield peak in the D_2-prepared sample, D, is positioned on a broad base, but is approximately the same position and width as the upfield peak in the *steady-state* samples (A–C).

As shown in Fig. 6, the saturation–recovery study of sample D reveals that different regions of the spectrum relax at different rates. The integrated intensity in the downfield region declines by about 30% when the delay between scans is decreased from 5 to 1 sec, whereas the upfield feature near 20 ppm decreases by over 70%. The integrated intensity of spectrum A corresponds to 3.0×10^{-5} g mol of ^{13}C.

The saturation–recovery study reveals variations in the T_1's of the different spectral features of sample D. The spin–echo spectra of this D_2-prepared, *converted*, Ru/SiO_2 sample, shown in Fig. 7, reveal that the different spectral features also have different T_2's. The downfield portion (~400 ppm) persists longer than other portions of the spectrum, indicating a longer T_2. The rate of decline of the upfield peak as a function of the delay to the echo is comparable to that of the *steady-state* samples in Fig. 4.

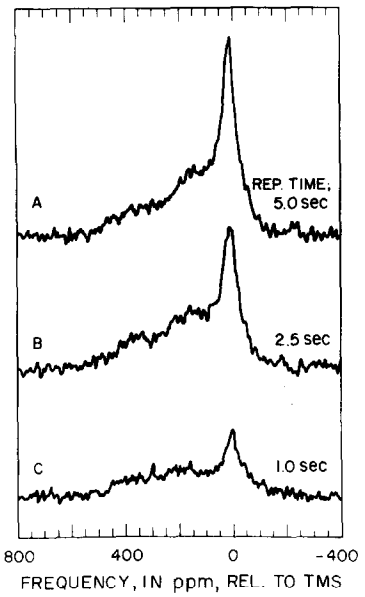

FIG. 6. Saturation–recovery study of a Ru/SiO_2 catalyst prepared by CO hydrogenation in D_2, then quenched after a He purge, to convert the adsorbed forms of carbon (Sample D). The ^{13}C NMR spectra were acquired at 295 K with intervals between successive scans of 5.0 sec (A), 2.5 sec (B), and 1.0 sec (C). Each spectrum is the summation of about 32,000 scans.

The absorption in the mid-range of the spectrum (200 to 50 ppm) decreases the most rapidly, such that the upfield and downfield peaks are nearly resolved to the baseline with a spin–echo delay of 0.3 msec.

The ^{13}C NMR spectra of the Ru/SiO_2 samples with *converted* carbon coverages exhibit a pronounced dependence on the hydrogen isotope. As shown in Fig. 8, replacing D_2 with H_2 causes the narrow upfield component to vanish into the broad base. The rate of decline of the spectral intensity as a function of the delay between scans (not shown) is comparable to that of the previous samples and indicates that the longest T_1 does not exceed about 3 sec. The integrated intensity of the spectrum represents 1.65×10^{-5} g mol of ^{13}C.

The spin–echo spectra in Fig. 8 are consistent with the trends observed in the spectra in Fig. 7. As before, the downfield portion does not decrease in intensity as rapidly as the other portions of the spectrum. In contrast, the intensity in the mid-range (200 to 50 ppm) decreases so as to reveal a separation between the downfield and upfield peaks in the echo at 0.2 msec. The upfield peak that appears in the echo at 0.2 msec is broader than the upfield peak in the Ru/SiO_2 sample prepared with D_2.

The relative areas and relaxation times of each overlapping feature in the ^{13}C NMR spectra of *converted* samples can be determined after each component is identified. This is presented under Discussion.

3. Titrated Ru/SiO_2 sample. The *titrated* Ru/SiO_2 sample contains only carbon that is resistant to reaction with D_2 after 2 hr at 463 K. The ^{13}C NMR spectrum of this sample,

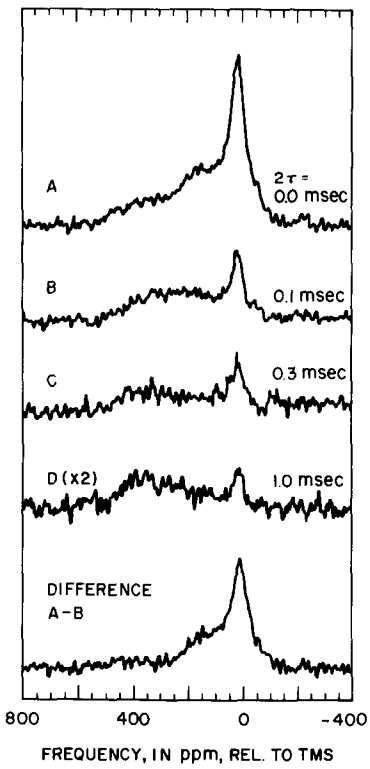

FIG. 7. Spin–echo study at 295 K of a Ru/SiO_2 catalyst prepared by CO hydrogenation in D_2, then quenched after a He purge, to convert the adsorbed forms of carbon (Sample D). The ^{13}C NMR spectra were obtained from a free-induction decay (A) and from the echoes stimulated by a 180° pulse 0.1, 0.3, and 1.0 msec after the 90° excitation. All spectra were acquired with a repetition time of 3 sec and represent about 20,000 scans each.

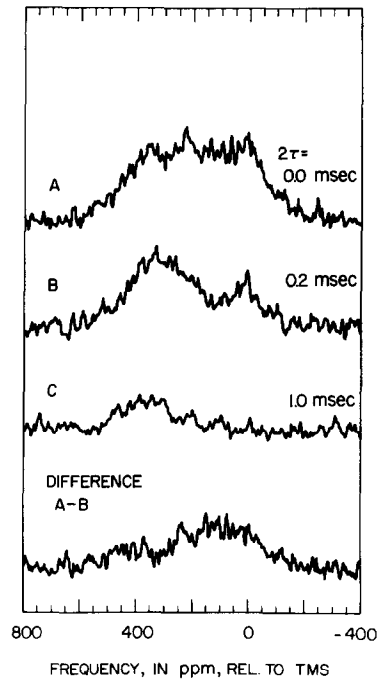

FIG. 8. Spin–echo study at 295 K of a Ru/SiO_2 catalyst with *converted* coverage, prepared as follows; methanation (in H_2), $^{13}CO/^{12}CO$ exchange, He purge, then quenched (Sample E). The ^{13}C NMR spectra were obtained from a free-induction decay (A) and from the echoes stimulated by a 180° pulse 0.2 and 1.0 msec after the 90° excitation. All spectra were acquired with a repetition time of 5 sec and represent about 64,000 scans each.

F, in Fig. 9 has a center of mass of 89 ± 15 ppm and has an integrated intensity that indicates 7.0×10^{-6} g mol of ^{13}C remain on the catalyst. Because the ^{13}C NMR signal is weak, the spectra require long measurement times; the spectrum in Fig. 9 is the result of 72 hr of acquisition. Consequently, the T_1 and T_2 of the lineshape were only estimated. The relative intensity of the spectrum measured with repetition times of 4 and 1 sec suggest T_1 is about 3 sec. The signal observed as an echo detected after a delay of 0.6 msec is about 10–20% that of the FID, which implies T_2 is approximately 0.3 msec.

Also shown in Fig. 9 is the ^{13}C NMR spectrum of 90% ^{13}C-enriched turbostratic graphite, obtained from an echo refocussed 0.010 msec after the 90° pulse. The ^{13}C NMR spectrum of graphite resembles that expected for axially symmetric shielding, since the carbon site has threefold symmetry (*17, 18*). It is unusual that the broadening varies across the spectrum. That is, the $\sigma_\perp$ component at about 20 ppm is distinct, but there is considerable tailing in the upfield (more positive) direction. We believe that the variation in broadening is due, in part, to the orientational dependence of the magnetic susceptibility of the bulk sample. The principal components of the shielding, obtained by fitting a broadened powder pattern, are $\sigma_\parallel = 251$ ppm and $\sigma_\perp = 20$ ppm.

4. Powdered ruthenium samples. The ^{13}C NMR spectra of Ru-powder catalysts with *steady-state* coverages (samples G and H) are shown in Fig. 10. The conditions used to prepare samples G and H were comparable to the conditions used for samples A and C, respectively, except the concentration of hydrogen and ^{13}CO were lowered

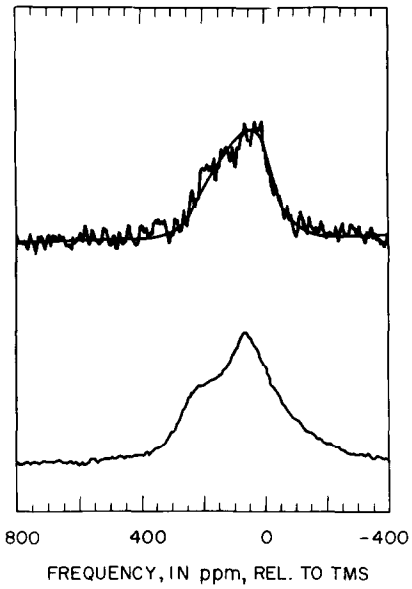

FIG. 9. ^{13}C NMR spectrum (top) at 295 K of a Ru/SiO_2 catalyst after methanation, followed by titration in D_2 for 2 hr (Sample F). A least-squares fit of a theoretical chemical shift powder pattern to the ^{13}C NMR spectrum of unreactive carbon is shown by the solid line through the upper spectrum. The spectrum is the accumulation of 65,000 scans at a repetition time of 4 sec. Shown below for comparison is the ^{13}C NMR spectrum of ^{13}C-enriched (91%) turbostratic graphite.

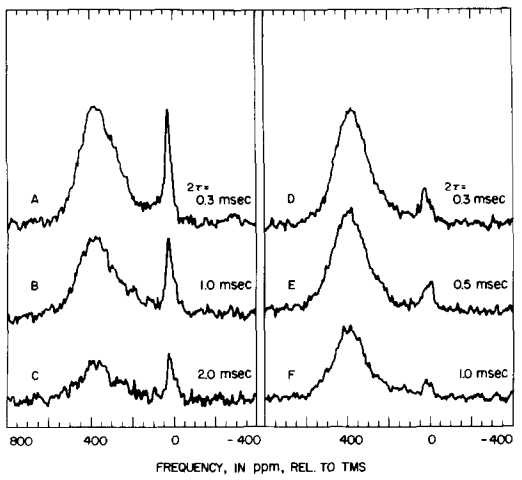

FIG. 10. Spin–echo study at 295 K of Ru-powder catalyst quenched after methanation and $^{13}CO/^{12}CO$ exchange (steady-state samples). Sample G (left) was prepared in D_2 and sample H (right) was prepared in H_2. These spectra were acquired with a repetition time of 5 sec; the spectra for sample G represent about 16,000 scans each and those for sample H represent about 32,000 scans each.

and the hydrogen : ^{13}CO ratio was reduced to 3.0. Although the ^{13}C NMR spectra of the Ru-powder samples comprise the two basic features shown in Figs. 2 and 5, there is a marked change in the relative intensities; the downfield peak is much larger and the upfield peak is smaller.

Although the spectral features in Fig. 10 are similar in shape to those of the Ru/SiO_2 samples in Figs. 2 and 5, there are subtle changes. The upfield peak in the D_2-prepared sample, G, is shifted by about 8 ppm to 28 ± 1 ppm and the line is about 40% more narrow; the Lorentzian half-width is 0.74 ± 0.05 kHz. The upfield peak in the H_2-prepared sample, H, is rather weak and thus does not offer an accurate description. However, it appears that the upfield peak is broader (half-width is 1.3 ± 0.2 kHz); it is not possible to determine if it too has shifted. Recall that the upfield peak in the spectra of the H_2-prepared, *steady-state* Ru/SiO_2 catalyst (sample C, Fig. 5) is the superposition of narrow and broad Lorentzian lineshapes. It is not possible to determine whether the upfield peak in spectrum C of Fig. 10 is a similar superposition.

Within experimental error, the lineshape of the downfield peaks in Fig. 10 are the same in the ^{13}C NMR spectra of the D_2-prepared and H_2-prepared Ru-powder catalysts. Furthermore, the shapes of the downfield peaks in Fig. 10 are similar to the downfield peaks of the Ru/SiO_2 samples; both peaks have a half-width of 4.4 ± 0.1 kHz and are centered at 375 ± 15 and 390 ± 15 ppm, for samples G and H, respectively.

The T_2's of the two peaks in the Ru-powder samples are independent of the hydrogen isotope and are longer than the T_2's measured with the Ru/SiO_2 samples. The T_2 of the downfield and upfield peaks are 1.5 and 1.3 msec on the H_2-prepared sample, respectively, and are both 1.4 msec on the D_2-prepared sample. Again, the intensity of each peak decreases exponentially with echo delay. Within experimental error, the linewidths and centers of mass do not change as the echo time is increased, as shown in Fig. 10.

The saturation–recovery experiment was not performed to measure the T_1's of the carbon species on the Ru-powder catalysts. However, if the T_1's are comparable to those of the Ru/SiO_2 samples, the spectra in Fig. 10 are not attenuated by saturation. The amount of ^{13}C on the Ru-powder catalysts is calculated from the intensities in spectra A and D (Fig. 10), corrected for the decay that occurred during the 0.3-msec delay to the echo. Both the D_2- and H_2-prepared *steady-state* Ru-powder samples contain 2.2×10^{-5} g mol of ^{13}C. The quantitative separation of the peaks is postponed until a discussion of the absorption in the range 200 to 50 ppm. However, the downfield peak at ~380 ppm constitutes about 80% of the D_2-prepared catalyst and about 90% of the H_2-prepared catalyst.

5. CO and CO_2 adsorbed on Ru/SiO_2. The ^{13}C NMR spectra of Ru/SiO_2 catalyst saturated with ^{13}CO and $^{13}CO_2$ at room temperature are shown in Fig. 11. Each spectrum contains a sharp peak at 124 ppm, which is interpreted as physically adsorbed and gas-phase CO_2 (7). The CO_2 in the sample of adsorbed CO was probably formed

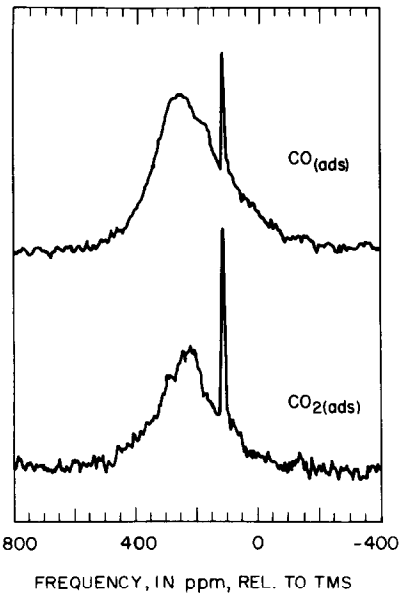

FIG. 11. ^{13}C NMR spectra 295 K of Ru/SiO_2 catalysts reduced in D_2, cooled to room temperature, and exposed to saturation coverages of ^{13}CO (Sample I, top) and $^{13}CO_2$ (Sample J, bottom). The spectrum of adsorbed ^{13}CO is the accumulation of 40,800 scans measured at intervals of 3 sec and the spectrum of adsorbed $^{13}CO_2$ is the sum of 28,500 scans acquired with a repetition time of 4 sec.

by the reaction with hydroxyl groups or residual oxygen on the catalyst. The width of the CO_2 peak, 200 Hz, is due to the exponential function applied to the free-induction decay to reduce the noise; the unperturbed linewidth is about 20 Hz. Thus, the presence of the CO_2 line demonstrates that the Ru/SiO_2 catalysts do not have inherent inhomogeneities, such as bulk magnetic susceptibility, which could contribute to the broadening in the spectra in Figs. 2–9.

The integrated intensity of the spectrum of adsorbed CO corresponds to 3.2×10^{-5} g mol of ^{13}C, which yields an estimated CO : surface Ru ratio of 0.84. Since this value is close to 1.0, we conclude that although T_1 was not measured, the ^{13}C signal is not significantly saturated by a repetition time of 3.0 sec. The center of mass of the spectrum of adsorbed CO is 221 ± 5 ppm. The magnitude of the broadening in the chemical shift powder pattern in Fig. 11 is similar to that of CO adsorbed on Al_2O_3-supported Rh (*19*). Also, the variation of the broadening across the powder pattern is typical of linear molecules such as terminally bonded carbonyls (*20*) or inorganic acetylides (*21*). That is, the inhomogeneity in shielding is larger for species oriented with symmetry axes nearly parallel to the field than for those species oriented perpendicular to the field. Thus, the upfield shoulder of the powder pattern of adsorbed CO, which is inherently small, is further smeared into the baseline by the strongest inhomogeneity-induced broadening. The principal components of the powder pattern of adsorbed CO, obtained from a least-squares fit to an inhomogeneity-compensated axially symmetric shielding, yield values of $\sigma_\perp = 317 \pm 15$ ppm and $\sigma_\parallel = 31 \pm 30$ ppm.

The integrated intensity of the spectrum of adsorbed CO_2 in Fig. 11 indicates the sample contains 2.3×10^{-5} g mol of ^{13}C, which is the same as the amount determined by volumetric uptake during the preparation of the sample. Thus, the ^{13}C NMR signal is not saturated by a repetition time of 4.0 sec. The center of mass of the chemically adsorbed CO_2 is 240 ± 10 ppm. A least-squares fit to a chemical shielding powder pattern yields $\sigma_{11} = 380 \pm 20$ ppm, $\sigma_{22} = 250 \pm 15$ ppm, and $\sigma_{33} = 75 \pm 20$ ppm.

IV. DISCUSSION OF RESULTS

A. ^{13}C NMR Spectra of Adsorbed CO and CO_2

The isotropic shift of adsorbed CO is 221 ± 5 ppm, which suggests that CO is bonded terminally to a Ru atom (*8–10, 20*). The anisotropy of the chemical shielding is about 350 ppm, which is typical of the anisotropy of terminal groups in transition metal carbonyls (380 ± 60 ppm) in the absence of intramolecular rearrangement (*20*). Thus, at room temperature CO is fixed at an on-

top site, relative to the time scale of the NMR measurement, about 0.1 msec.

The amount of CO_2 adsorbed on the Ru/SiO_2 sample J, determined from pressure–volume measurements, is 1.7×10^{-3} g mol CO_2/g Ru, which corresponds to 15% of a Ru monolayer. This is roughly 10-fold higher than the coverage reported previously for CO_2 adsorption at room temperature on a Ru/SiO_2 catalyst (*22*). Since CO_2 adsorption was found to be an activated process (*22*), the higher coverage reported here is probably a result of the long equilibration time used (14 hr). All the CO_2 on the catalyst surface at room temperature is assumed to be molecular CO_2, based on the observation that temperatures above 350 K are required for dissociative adsorption on Ru/SiO_2 (*22*).

The ^{13}C NMR spectrum of adsorbed CO_2 is unlike that reported previously for CO_2 on oxide surfaces. For example, CO_2 adsorbed on a zeolite has a spectrum with an isotropic shift similar to that of the gas-phase CO_2 (*23*). For submonolayer coverages, the shape of the powder pattern suggests that the CO_2 molecules are rigidly adsorbed and have axial symmetry; the upfield components are degenerate, like that of CO. The observed spectrum of CO_2 on Ru/SiO_2 is different in two respects. The isotropic shift has moved downfield by over 115 ppm to 240 ppm, typical of bonding to metals, and the powder pattern has three distinct components, indicating nonaxial symmetry at the carbon atom. These observations are consistent with the structure proposed for CO_2 ligands on Ni and Rh (*24*):

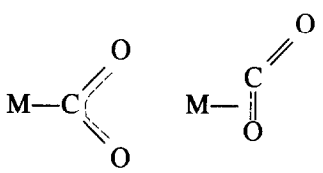

A bidentate species bonded to Ru through the two oxygen atoms, such as reported for the reaction of ruthenium hydride with CO_2 (*25*), is consistent with the lack of axial symmetry, but would be predicted to have an isotropic shift similar to that of esters; 170 ppm.

B. Interpretation of Unreactive Carbon

The lineshape of the unreactive carbon is well fit by a broadened, chemical shift powder pattern, as shown in Fig. 9. The theoretical fit, restricted to an axially symmetric shielding ($\sigma_{22} = \sigma_{33}$) yields values of $\sigma_\parallel = 245 \pm 30$ ppm and $\sigma_\perp = 16 \pm 20$ ppm, with a homogeneous broadening of 2.6 kHz (51 ppm). Note that the isotropic shift and principal shielding parameters of unreactive carbon are consistent with those of graphite ($\sigma_\parallel = 251$ and $\sigma_\perp = 20$ ppm). Furthermore, both powder patterns have the uncommon feature that $\sigma_\parallel$ lies downfield of $\sigma_\perp$. To our knowledge, this has been observed for ^{13}C in only two other cases. The ^{13}C NMR spectrum of WC, which is composed of alternate hexagonal layers of W and C, has principal components at $\sigma_\parallel = 348$ ppm and $\sigma_\perp = 286$ ppm (*21*). The other case is that of some esters (*e.g.*, dimethyl oxalate, acetic anhydride, and dimethyl carbonate) for which $\sigma_\perp$ is about 230 to 280 ppm and $\sigma_\perp$ is 110 to 115 ppm (*26*). Finally, the T_2 of the unreactive carbon is estimated to be less than 0.3 msec. The calculated second moment of the ^{13}C–^{13}C dipolar coupling for a two-dimensional graphitic plane, averaged over all orientations, is 9.5 kHz^2, which corresponds to a T_2 of 0.05 msec. Thus, from the anisotropy and orientation of its ^{13}C NMR powder pattern and its estimated T_2, we interpret the unreactive carbon as a graphitic overlayer.

Unfortunately, nothing can be stated about the thickness of the graphitic overlayer or its interactions with the catalyst. The coupling between layers of turbostratic graphite is weaker than that of highly oriented pyrolytic graphite; the interplanar separation is typically 3.44 Å compared to 3.35 Å (*12, 13*). Theoretical models suggest that the electron energy bands near the Fermi level for turbostratic graphite can be represented by a two-dimensional lattice

(*12*). Consequently, we expect that the ^{13}C NMR spectrum of turbostratic graphite is determined primarily by in-plane interactions and is insensitive to the layers above and below. Therefore, the similarity between the spectrum of turbostratic graphite and unreactive carbon cannot be interpreted as evidence that the unreactive carbon exists as three-dimensional structures.

C. Interpretation of the Downfield ^{13}C NMR Peak

The downfield peak represents from 10 to 20% of the integrated area in the Ru/SiO_2 samples with *steady-state* coverages and its relative intensity increases in the spectra of samples with *converted* coverages. These results parallel the surface population of the C_α species, as determined by transient response methods (*1*). Based on this, the downfield peak was assigned to C_α (*3*). We present here an interpretation of the C_α species, based on the center of mass, linewidth, and T_2 of its ^{13}C NMR peak.

The centers of mass of the downfield peaks in the Ru/SiO_2 and Ru-powder samples with *steady-state* coverages are approximately 380 ppm. This is considerably downfield of the normal range of isotropic shifts of organic compounds (225 to 0 ppm) (*7*), but lies within the range of organometallic compounds (*8–10*) and transition metal carbides (*21, 27*). The only organometallic species reported with ^{13}C isotropic shifts that correspond to the C_α peak are the terminal carbenes, which range from about 375 to 275 ppm (*28*). The range of ^{13}C isotropic shifts of carbides in carbidocarbonyl complexes extend further downfield, from about 485 to 265 ppm (*27*). In particular, the carbide resonances in two ruthenium complexes, $[Ru_6C(CO)_{16}]^{2-}$ and $(CH_3CN)_2Cu_2Ru_2C(CO)_{16}$ are reported at about 459 ppm (*27*). The carbides in interstitial transition-metal compounds exhibit a similarly large range of isotropic shifts. The ^{13}C resonances of Group IVB, VB, and VIB metal carbides span the range from 580 to 200 ppm (*21*). Unfortunately, although a stable form of RuC has been reported (*29*), no ^{13}C NMR data are available. In summary, the center of mass of the C_α peak is consistent with the isotropic shifts of terminal carbenes and transition-metal carbides. To resolve the interpretation, it is necessary to consider differences in nuclear dipolar couplings.

A terminal carbene and a carbide have different nuclear dipole–dipole couplings by virtue of their proximity to other nuclei. The carbene carbon is bonded to a Ru atom and to two other atoms each of which may be a carbon or hydrogen atom. Because of the low gyromagnetic ratios and low isotopic abundances of the magnetically active isotopes of ruthenium, ^{99}Ru and ^{101}Ru, the Ru atom would contribute very little (0.02 G^2) to the second moment of the ^{13}C spectrum of a carbene. The major contribution would be from carbon and hydrogen bonded to the carbene. Some representative second moments, calculated from the Van Vleck equation (*5, 6*) are: $Ru{=}C^*H_2$, (190 G^2); $Ru{=}C^*D_2$, (12.0 G^2); $Ru{=}C^*H(C_nH_{2n+1})$, (9.7 G^2); $Ru{=}C^*D(C_nD_{2n+1})$, (7.7 G^2); and $Ru{=}C^*(C_nH_{2n+1})_2$, (3.4 G^2). Only the first coordination shell need be considered in this estimate, since the second moment drops off as r^{-6}, and because the free ends of species such as $Ru{=}C^*(C_nH_{2n+1})_2$ probably librate freely which decreases the couplings. The first coordination shell of a carbide species consists exclusively of Ru atoms. The principal nuclear dipolar couplings are to species at neighboring sites on the Ru surface or within the Ru particle; ^{13}C nuclei at adjacent threefold sites on the surface yield a second moment of 1.6 G^2 and ^{13}C nuclei in adjacent interstitial voids in RuC yield a second moment of about 0.5 G^2.

The ^{13}C NMR spectra of C_α have halfwidths that range from 3.1 to 4.4 kHz (2.7 to 3.8 G). Many phenomena contribute to the width of the peak. To estimate the contribution from nuclear dipolar interactions, we consider the magnitude of T_2. In gen-

eral, homonuclear ^{13}C–^{13}C coupling will result in a T_2 equal to the reciprocal of the square root of its contribution to the second moment. Thus the predicted T_2 for the carbene carbon in $Ru{=}C^*(C_nH_{2n+1})_2$ is 0.08 msec. The relation between heteronuclear couplings (e.g., ^{13}C—^1H) and T_2 is more complex and depends in part on the rate of fluctuation of the second spin (i.e., ^1H) as the result of other ^1H nuclei (*30*). Using the theoretical approach described in reference (*30*), we estimate the T_2's of the $Ru{=}C^*H_2$, $Ru{=}C^*D_2$, $Ru{=}C^*H(C_nH_{2n+1})$, and $Ru{=}C^*D(C_nD_{2n+1})$ species to be less than 0.12 msec. To calculate these values of T_2, it was assumed that the time constant for rotation or diffusion between sites for a terminal carbene is longer than the echo delay (about 1 msec). Since there has been no report of fluxional motion of bridging carbenes in organometallic clusters (*28*), it is expected that terminal carbenes would be fixed.

The T_2's of the C_α peaks (see Table 3) are considerably longer than the T_2's predicted for nonreorienting, terminal carbene species. In other words, the C_α species has considerably less nuclear dipolar coupling than carbene species. Moreover, the T_2's are not correlated with the choice of hydrogen isotope. This leads us to conclude that the C_α species cannot be attributed to a terminal carbene, and must therefore be interpreted as a carbidic carbon coordinated to Ru atoms.

With only the isotropic shifts and T_2's, we cannot determine if the carbon atom is located on the surface of Ru particles or in interstitial voids. This point is supported by noting that the isotropic shifts of carbon atoms in carbidocarbonyl clusters are insensitive to the coordination of the carbide carbon. For example, the relatively exposed carbon atom in $[Fe_4C(CO)_2]^{2-}$ resonates at 478 ppm, while the encapsulated carbon atom in $[Fe_6C(CO)_{16}]^{2-}$ resonates at 485 ppm (*27*).

The ^{13}C NMR spectra of C_α species have half-widths of about 3.1 to 4.4 kHz, of which only about 0.10 to 0.16 kHz can be attributed to nuclear dipolar interactions. The principal broadening is not likely to be orientational anisotropy of the chemical shielding; the C_α peaks do not resemble a generalized powder pattern and the width is greater than the anisotropy observed in similar environments. For example, the ^{13}C chemical shift powder pattern for WC,

TABLE 3

Summary of ^{13}C NMR Parameters

Sample	Downfield peak (C_α)				Upfield peak (C_{β_1} and C_{β_2})			
	Center of mass[a]	Linewidth[b] (kHz)	T_2 (msec)	T_1 (sec)	Center of mass[a]	Lindwidth[c] (kHz)	T_2 (msec)	T_1 (sec)
A. Ru/SiO_2; Steady state; D_2	390 ± 15	3.1 ± 0.3	—	1.1	19 ± 1	1.16 ± 0.03	—	3.3
B. Ru/SiO_2; Steady state; D_2	—	—	—	—	14 ± 1	1.10 ± 0.03	0.80	4.7
C. Ru/SiO_2; Steady state; H_2	380 ± 25	4.4 ± 0.4	2.3	—	C_{β_1}; 10 ± 4 (50%) C_{β_2}; 18 ± 2 (50%)	3.9 ± 0.3 1.23 ± 0.03	0.20 0.34	—
D. Ru/SiO_2; Converted; D_2	320 ± 20	5.9 ± 0.3	1.0	1.0	15 ± 3	1.26 ± 0.05	0.58	3.2
E. Ru/SiO_2; Converted; H_2	310 ± 20	6.2 ± 0.4	1.1	~1.0	10 ± 10	3.5 ± 0.2	0.25	~1.0
G. Ru; Steady state; D_2	375 ± 15	4.4 ± 0.1	1.4	—	28 ± 1	0.74 ± 0.05	1.4	—
H. Ru; Steady state; H_2	390 ± 15	4.4 ± 0.1	1.5	—	23 ± 5	1.3 ± 0.2	1.3	—

[a] In ppm, relative to TMS.
[b] Half width at maximum slope of a Gaussian function fit to the peak.
[c] Half width at half-height of a Lorentzian function fit to the peak.

which is isomorphous with the structure reported for RuC (*29*), has principal components of $\sigma_{\parallel} = 348$ ppm and $\sigma_{\perp} = 286$ ppm, for an overall anisotropy of 62 ppm (*21*). Although the isotropic shift of the ^{13}C NMR spectrum of carbides of Ru may be shifted from that of WC, the spectrum of RuC would probably have a comparable shielding anisotropy. Such a peak width is much less than that observed for the C_α peaks (*cf.* Fig. 10).

We propose, therefore, that the width of the C_α peak is caused by a distribution of isotropic shifts due to variation in the geometry of the carbide sites. If the variation in each site is the net result of many defects, the central limit theorem applies and one predicts a Gaussian lineshape, as is observed. Similar lineshapes are obtained for the ^{13}C NMR spectra of interstitial transition-metal carbides, where the source of inhomogeneity is the lattice distortions caused by vacancies. For example, TiC has a Gaussian lineshape of half-width 3.6 kHz, although the contribution from heteronuclear dipolar coupling is only 0.27 kHz (*21*).

D. Interpretation of the Upfield ^{13}C NMR Peak

In the spectra of *steady-state* Ru/SiO_2 samples, the upfield peak represents 80 to 90% of the total integrated area. When a *steady-state* sample is purged with an inert gas prior to quenching, the intensity of the upfield peak decreases, and there is a concurrent growth in the intensity of the downfield peak. This pattern closely parallels the changes in the coverages of C_α and C_β determined from transient-response experiments (*1*), and leads to the assignment of the upfield peak to C_β (*3*).

Comparison of the upfield peaks of similar H_2- and D_2-prepared *steady-state* samples suggests that the peak is composed of two components and that each component corresponds to a hydrogenated carbon. That is, it was noted that the upfield peak in Fig. 5 (sample C; H_2-prepared, *steady-state*) is best described as the sum of two Lorentzian lines: a narrow component centered at 18 ± 2 ppm with a half-width of 1.23 ± 0.03 kHz and a broader component centered at 10 ± 4 ppm with a half-width of 3.9 ± 0.3 kHz. Since the two components are separated by ~8 ppm (0.4 kHz) it is not possible to determine the individual widths in the spectra of the D_2-prepared samples, and thus one cannot precisely determine the contribution of ^{13}C–^{2}D (or ^{13}C–^{1}H) dipolar coupling to the linewidths of the individual components. However, the broad component of the upfield peak in Fig. 5, designated hereafter as C_{β_1}, is at least a factor of 3.4 broader than that of D_2-prepared samples. Since replacing ^{2}D with ^{1}H increases ^{13}C–hydrogen dipolar broadening by a factor of 4.0, one concludes that the broadening in the C_{β_1} component of the upfield peak is due mostly to nuclear dipolar coupling to hydrogen. The ^{13}C–hydrogen coupling in the narrow component, designated C_{β_2}, is better revealed by the decrease in its T_2. The composite T_2 of the upfield peak in a D_2-prepared catalyst (sample B) is 0.8 msec. The T_2 of the C_{β_2} component decreases to 0.34 msec for the H_2-prepared sample. Therefore, both components of the upfield peak correspond to hydrogenated carbon. This is consistent with the observation of C–H stretching vibrations in the infrared spectra of Ru/SiO_2 catalysts after sustained CO hydrogenation (*31*).

The centers of mass of the components of the upfield peak are consistent with hydrogenated carbon and furthermore restrict the assignment to paraffinic species. The centers of mass lie in the range 28 to 10 ppm, which is the range observed for carbon with sp^3 hybridization, e.g., saturated hydrocarbons (*7*). Also, the α-carbon of an alkyl ligand resonates within this range (*8–10*). Carbons with sp^3 hybridization bonded to oxygen (alcohols, esters) generally lie upfield in the range 90 to 60 ppm and thus are not candidates for the upfield peak.

The low-temperature spectra of sample A (D_2-prepared, *steady-state*) further show that the upfield peak is composite. The

peak measured at 110 K is best represented by the superposition of a Gaussian lineshape and a Lorentzian lineshape. From a least-squares fit, it is determined that the Gaussian peak has a center of mass of 26 ppm and a half-width of 5.3 kHz. The Lorentzian lineshape is centered at 9 ppm and has a half-width of 2.0 kHz. The ratio of the two components is approximately 50 : 50, which agrees with the relative intensities of the components of the H_2-prepared sample (B). The Lorentzian shape of the narrow component of the upfield peak, interpreted as C_{β_2}, suggests that although the motional averaging has decreased, it is not arrested. Conversely, the Gaussian lineshape of the broad component, interpreted as C_{β_1}, suggests that at 110 K the motional averaging is quenched. However, the half-width exceeds that predicted for a methylene carbon in a deuterated linear alkyl group, 4.3 kHz. The cause of the excess broadening is not known. It is expected that there is little contribution from orientational anisotropy of the chemical shift since this is only 25 to 30 ppm for methylene carbons (*17*). The result of convoluting a Gaussian peak of half-width 4.3 kHz with a powder pattern with an anisotropy of 30 ppm is indistinguishable from a Gaussian lineshape of halfwidth 4.3 kHz.

A rough estimate of the activation energy of the motion of the C_β species can be obtained from the increase in linewidth that accompanies the decrease in temperature. From the Arrenhius plot in Fig. 12, the slope of the high-temperature segment indicates that the activation energy is 0.6 ± 0.04 kcal/mol. This is a rough estimate for two reasons. First, this is an average activation energy of two species shown to have different motional properties. Second, the linewidths contain contributions from differences in isotropic shifts, which may be significant at near room temperature. The individual activation energies could be obtained by performing spin–echo experiments on a H_2-prepared sample at each temperature, decomposing the spectra into

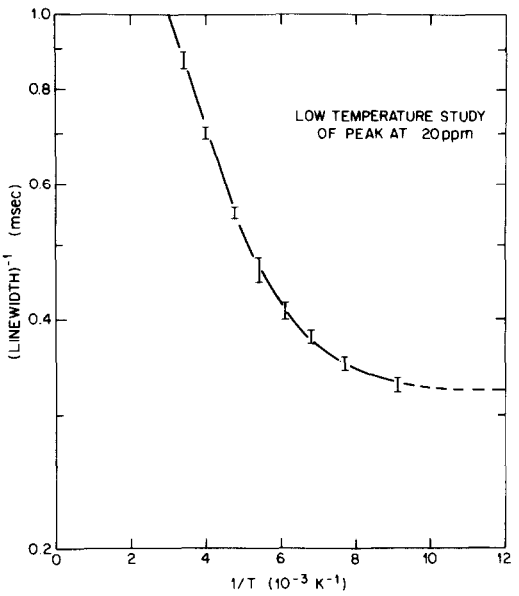

FIG. 12. The Lorentzian linewidths of the spectra of a Ru/SiO_2 catalyst in Fig. 3 as a function of temperature.

C_{β_1} and C_{β_2}, and then plotting the T_2's versus the inverse temperature.

It is noted that the interpretation of the upfield peak differs from that proposed in our initial ^{13}C NMR study (*3*). It was suggested there that the upfield peak be assigned to C_β, which was interpreted as a nonhydrogenated carbon bonded to silicon atoms in the silica support. The present observation of an upfield peak for both Ru/SiO_2 and Ru powder indicates that at least one of the species giving rise to the upfield peak must be associated with the Ru metal.

E. Distribution of Carbonaceous Species

Using the proposed interpretations for the four forms of nonoxygenated carbon on the catalysts, we can now resolve the peaks in the ^{13}C NMR spectra that were severely overlapped, such as the spectra of the *converted* samples (Figs. 6–8). The following functional forms were shown earlier to describe the ^{13}C NMR spectrum of each component: C_α is a Gaussian, the unreactive carbon is a broadened chemical shift powder pattern (see Fig. 9), and the upfield peak is a Lorentzian. Although the upfield

peak is the superposition of two components, it is not possible to resolve the individual peaks, except in samples prepared with H_2 or in spectra measured at temperatures below 165 K. Thus, we decompose all the spectra with a seven-parameter least-squares fit. The seven parameters are the center of mass, linewidth, and intensity of the Gaussian C_α peak, the center of mass, linewidth, and intensity of the Lorentzian upfield peak, and the intensity of the powder pattern for the unreactive carbon. An illustration of the result of this procedure is shown in Fig. 13 for the *converted* Ru/SiO_2 samples D and E.

The quantities of each species on the Ru/SiO_2 catalysts (samples A–F) were determined from the ^{13}C NMR spectra measured as FID's and with the longest delays between scans. The ^{13}C NMR spectra of Ru powders (samples G and H) could not be measured as FID's, so the echoes at 2τ = 0.3 msec were analyzed and the quantities

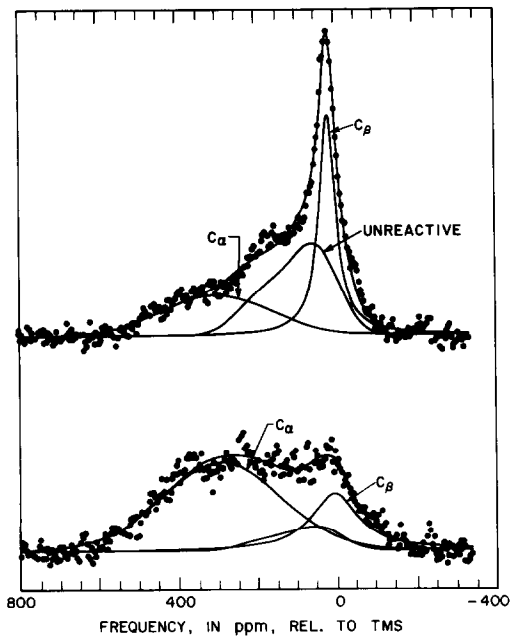

FIG. 13. Separation of the ^{13}C NMR spectra of the *converted* Ru/SiO_2 samples D, prepared in D_2 (top), and E, prepared in H_2 (bottom), by a least-squares fit to three components: a Gaussian downfield peak, a chemical shift powder pattern for the unreactive carbon, and a Lorentzian upfield peak.

were extrapolated to $2\tau = 0$ (i.e., a FID), by the T_2's. The surface populations are summarized in Table 2 and the ^{13}C NMR parameters of the downfield and upfield peaks are in Table 3. For samples A, B, C, and D, all of which were prepared on Ru/SiO_2, the ratios of $C_\alpha/(C_\alpha + C_\beta)$ determined by titration are 0.19, 0.05, 0.14, and 0.50, respectively. The corresponding values obtained from NMR spectra are 0.16, 0.05, 0.17, and 0.40. The close agreement between the values obtained by titration and NMR supports the assignment of the downfield and upfield peaks to C_α and C_β, respectively.

While the agreement in the values of $C_\alpha/(C_\alpha + C_\beta)$ determined by titration and NMR is quite good, the agreement in the measurements of total carbon on the catalysts is not good. The amount of carbon detected by NMR is consistently greater than that detected by titration. The exact reasons for this are not known.

In contrast to the good agreement between the ratios of $C_\alpha/(C_\alpha + C_\beta)$ on Ru/SiO_2 determined by titration and NMR spectroscopy, ratios for Ru powder are poorly correlated. For *steady-state* Ru powder samples (G and H), the ratio $C_\alpha/(C_\alpha + C_\beta)$ is 0.015 and less than 0.017 determined by titration, and 0.86 and 0.91 determined from NMR. The reasons for the discrepancy may be twofold. First, the resolution of C_α and C_β by titration is quite difficult and as a consequence a part of the total carbon identified as C_β may be C_α. Second, the C_α and C_β peaks in the NMR spectra may be artificially attenuated, since the T_1's were not measured. To correct for the incomplete approach to equilibrium, T_1's measured for carbon species on Ru/SiO_2 were used. If the T_1's for carbon on Ru powder are significantly different, the determinations of C_α and C_β from the saturation–recovery spectra will be in error.

We also note that the total amount of carbon on Ru powder determined from titration is an order of magnitude higher than that observed by NMR. This is likely due to

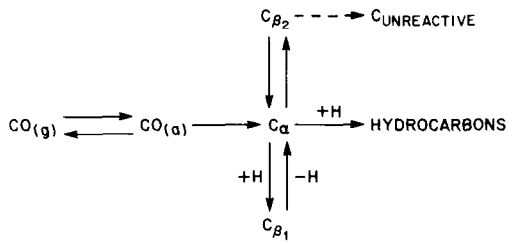

FIG. 14. Proposed scheme for the interconversion of species adsorbed on the ruthenium catalyst during steady-state methanation.

the attenuation of the NMR signal caused by the impedance mismatch to the probe and the attention of the rf signal caused by the bulk conductivity of the Ru powder.

The different adspecies observed by ^{13}C NMR can be related to one another in the manner illustrated in Fig. 14. The network presented here is similar to that proposed earlier by Winslow and Bell (*1*). Adsorbed CO dissociates to produce C_α, the primary intermediate from which all primary hydrocarbons are formed (*1, 2*). The C_{β_1} and C_{β_2} species are shown to derive from C_α. The formation of unreactive, graphitic carbon from C_{β_2} is speculative and is proposed primarily on the basis of the results shown in Fig. 13, which demonstrate that purging with an inert gas primarily depletes the C_{β_2} peak, concomitant with the increase of C_α and unreactive carbon. In the previous discussion, the C_{β_1} and C_{β_2} species were differentiated primarily by motional properties. The selective depletion of C_{β_2} with regard to C_{β_1} suggests that the species are distinct. That is, C_{β_1} and C_{β_2} are not simply the opposite ends of an alkyl chain attached to the catalyst, with C_{β_2} as the freely reorienting ends.

V. SUMMARY

^{13}C NMR spectroscopy has been used to characterize the forms of adsorbed carbon present on ruthenium catalysts following CO hydrogenation. Three distinct forms were identified, designated C_α, C_β, and unreactive carbon. Furthermore, it is shown that the C_β species can be separated into species C_{β_1} and C_{β_2}. The structure and motional properties of these species were established from the characteristics of the NMR peaks, i.e., position, linewidth, and lineshape. The reactivity of the individual species with hydrogen were established through independent experiments.

C_α reacts rapidly with hydrogen and is the principal form of carbon responsible for the synthesis of hydrocarbons from CO and H_2. It is characterized by a Gaussian NMR peak centered at 380 ppm with a half-width of 3.1 to 4.4 kHz. Based on its isotropic shift, spin–spin relaxation time, and linewidth, C_α is interpreted as carbidic carbon atoms distributed in a variety of sites on or below the metal surface.

The C_β species react less rapidly with hydrogen than does C_α. The NMR spectra of C_β at room temperature have centers of mass that range from 10 to 28 ppm and are the superposition of two components, designated C_{β_1} and C_{β_2}. For the Ru/SiO_2 samples studied here, the ratio of C_{β_1} to C_{β_2} after steady-state methanation is about 50 : 50. The center of mass and line broadening caused by replacing D_2 with H_2 in the preparation suggest that both components are paraffinic species. C_{β_1} and C_{β_2} have different motional properties. C_{β_1} reorients less and its motion is quenched at 110 K. C_{β_2} is more motionally averaged and is not quenched at 110 K. Purging a Ru/SiO_2 catalyst with an inert gas selectively removes the C_{β_2} component of the C_β peak.

An unreactive carbon species remained on the catalyst surface following the reaction of CO and H_2, and subsequent H_2 reduction to remove all reactive forms of carbon. The unreactive carbon exhibits a broadened chemical shift powder pattern similar to that of turbostratic graphite.

Based on the results of transient-response studies and ^{13}C NMR, it is concluded that C_α is formed via the dissociation of adsorbed CO. C_{β_1} and C_{β_2} derive from C_α. The available evidence suggests the C_{β_2} may be the precursor to unreactive carbon.

ACKNOWLEDGMENTS

The iron contents of the catalyst materials were provided by R. Fiato and the X-ray diffraction of the turbostratic graphite was measured by A. Lovinger. Discussions with D. C. Douglass provided invaluable information for the analysis of the NMR data. This work was supported in part by the Division of Chemical Sciences, Office of Basic Energy Sciences, U.S. Department of Energy under Contract DE-AC03-76SF0098.

REFERENCES

1. Winslow, P., and Bell, A. T., *J. Catal.* **86,** 158 (1984).
2. Winslow, P., and Bell, A. T., *J. Catal.* **91,** 142 (1985).
3. Duncan, T. M., Winslow, P., and Bell, A. T., *Chem. Phys. Lett.* **102,** 163 (1983).
4. Duncan, T. M., and Dybowski, C., *Surf. Sci. Rep.* **1,** 157 (1981).
5. Slichter, C. P., "Principles of Magnetic Resonance," 2nd ed. Springer, New York, 1978.
6. Abragam, A., "The Principles of Nuclear Magnetism." Oxford Univ. Press, London, 1961.
7. Stothers, J. B., "Carbon-13 NMR Spectroscopy." Academic Press, New York, 1972.
8. Jolly, P. W., and Mynott, R., *Adv. Organometall. Chem.* **19,** 257 (1981).
9. Pregosin, P. S., *in* "Annual Reports on NMR Spectroscopy" (G. A. Webb, Ed.), Vol. 11A, p. 227. Academic Press, New York, 1981.
10. Mann, B. E., and Taylor, B. F., "^{13}C NMR Data for Organometallic Compounds." Academic Press, New York, 1981.
11. McBrierty, V. J., and Douglass, D. C., *Phys. Rep.* **63,** 62 (1980).
12. Spain, I. L., "Chemistry and Physics of Carbon" (P. L. Walker, Jr. and P. A. Thrower, Eds.), Vol. 16, p. 119. Dekker, New York, 1981; and references therein.
13. Ubbelohde, A. R., and Lewis, F. A., "Graphite and Its Compounds." Oxford Univ. Press (Clarendon), London/New York, 1960.
14. (a) Franklin, R., *Acta Crystallogr.* **4,** 253 (1951); (b) Ebert, L. B., Mills, D. R., and Scanlon, J. C., *Mater. Res. Bull.* **17,** 1319 (1982).
15. Cant, N. W., and Bell, A. T., *J. Catal.* **73,** 257 (1982).
16. Dalla Betta, R. A., *J. Catal.* **34,** 57 (1974).
17. Mehring, M., "Principles of High Resolution NMR in Solids," 2nd ed. Springer-Verlag, New York, 1983.
18. Haeberlen, U., "High Resolution NMR in Solids: Selective Averaging" (Suppl. 1 to Advances in Magnetic Resonance). Academic Press, New York, 1976.
19. Duncan, T. M., Yates, Jr., J. T., and Vaughan, R. W., *J. Chem. Phys.* **73,** 975 (1980).
20. Gleeson, J. W., and Vaughan, R. W., *J. Chem. Phys.* **78,** 5384 (1983).
21. Duncan, T. M., manuscript in preparation.
22. Zagli, E., and Falconer, J. L., *J. Catal.* **69,** 1 (1981).
23. (a) Stejskal, E. O., Schaefer, J., Henis, J. M. S., and Tripodi, M. K., *J. Chem. Phys.* **61,** 2351 (1974); (b) Sefcik, M. D., Schaefer, J., and Stejskal, E. O., *in* "Magnetic Resonance in Colloid and Interface Science" (H. A. Resing and C. G. Wade, Eds.), p. 109. Amer. Chem. Soc. Symp. Ser. 34, Amer. Chem. Soc., Washington, D.C., 1976.
24. Darensbourg, D. J., and Kudaroski, R. A., *Adv. Organometall. Chem.* **22,** 129 (1983).
25. Kolomnikov, I. S., Gusev, A. I., Aleksandrov, G. G., Lobeeva, T. S., Struchkov, Yu. T., and Vol'pin, M. E., *J. Organometall. Chem.* **59,** 349 (1973).
26. Pines, A., Gibby, M. G., and Waugh, J. S., *Chem. Phys. Lett.* **15,** 373 (1972).
27. Bradley, J. S., *Adv. Organometall. Chem.* **22,** 1 (1983).
28. Herrmann, W. A., *Adv. Organometall. Chem.* **20,** 159 (1982).
29. (a) Kempter, C. P., and Nadler, M. R., *J. Chem. Phys.* **33,** 1580 (1960); (b) Kempter, C. P., *J. Chem. Phys.* **41,** 1515 (1964).
30. Reimer, J. A., and Duncan, T. M., *Phys. Rev. B: Condens. Matter* **27,** 4895 (1983).
31. Winslow, P. W., and Bell, A. T., unpublished results.